Tunable Ultranarrowband Grating Filters in Thin-Film Lithium Niobate

Alessandro Prencipe, Mohammad Amin Baghban, and Katia Gallo*

Read Online

ACCESS | Metrics & More | Article Recommendations | Supporting Information

ABSTRACT: Several applications in modern photonics require compact on-chip optical filters with a tailored spectral response. However, achieving subnanometric bandwidths and high extinction ratios is particularly challenging, especially in low-footprint device formats. Phase-shifted Bragg gratings implemented by the sidewall modulation of photonic nanowire waveguides are a good solution for on-chip narrowband operation with reasonable requirements in fabrication and scalability. In this work we report on their implementation and optimization in thin film lithium niobate, a photonic platform that affords reconfigurability by exploiting electro-optic effects. The phase-shifted Bragg grating filters have a footprint smaller than 1 μm × 1 mm and operate at telecom wavelengths, featuring extinction ratios up to 25 dB. We demonstrate transmission bandwidths as narrow as 14.4 pm ($Q = 1.1 \times 10^5$) and 8.8 pm ($Q = 1.76 \times 10^5$) in critically coupled structures and multiwavelength Fabry−Perot configurations, respectively, in full agreement with theoretical predictions. Moreover, by taking advantage of the strong electro-optic effect in lithium niobate, in combination with the tight light confinement of nanophotonic wires and the ultranarrow spectral resonances of optimized grating structures, we demonstrate an electric tunability in peak wavelength and transmission of 25.1 pm/V and 2.1 dB/V, respectively, and a 10.5 dB contrast at CMOS voltages. The results pave the way for reconfigurable narrowband photonic filters with a small footprint and low consumption, to be exploited toward on-chip quantum and nonlinear optics, as well as optical sensing and microwave photonics.

**KEYWORDS:** *Bragg grating, microcavity, nanophotonics, reconfigurable photonics, lithium niobate, electro-optics*
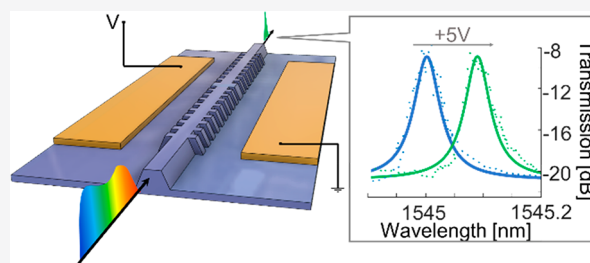
Integrated optical filters are essential components for a wide variety of applications,[1,2] encompassing photonic and microwave signal processing,[3,4] lasers,[5,6] telecom systems,[7−9] sensing,[10,11] and quantum optics.[12] Electrical tunability is an additional attractive feature, typically achieved by means of thermal, strain or carrier injection in optical fibers or silicon photonic circuits.[4,13] However, these approaches may suffer from high power consumption and introduce additional optical losses, motivating alternative solutions based on materials with a strong Pockels electro-optic response, such as lithium niobate (LN). Recent advances in LN nanophotonics allow the implementation of filters and resonators in various integrated optics architectures, namely, sidewall-modulated nanowire waveguides,[14−20] photonic crystal nanobeams,[21,22] microrings and racetrack resonators.[23−27] At telecom wavelengths, record quality factors have been achieved in ultralow-loss racetrack resonators, realized with 2.4 μm-wide rib waveguides in LN on insulator (LNOI).[24] For electro-optic applications, somewhat narrower waveguides ($w_0 \sim 1.1−1.5$ μm) are generally preferred, yielding $Q \sim 7 \times 10^5$.[25,26] The quoted Q factors for the above 2D resonator architectures provide a measure of the spectral linewidths for their operation as notch filters in transmission. Their operation as passband filters requires additional add/drop coupling structures[27] and further engineering to minimize at the same time the transmission

bandwidth and the power penalty of the filter.[28] Record results have been achieved in this case with Si-LN resonators exhibiting $Q \sim 1.2 \times 10^5$.[27] However, the heterogeneous configuration does not make the most effective use of the electro-optic (EO) effect of LN, restricting the wavelength tunability of such filters to values of few pm/V, well below those of monolithic LN devices.[23,27] 1D photonic crystal cavities ideally take advantage of the strong EO response of LN ($r_{33} = 33$ pm/V)[29,30] and provide high-contrast index modulations in ultrasmall device footprints. Moreover, by allowing engineering of the free spectral range (FSR), they can afford singly resonant or single-sideband operation, appealing for, for example, quantum optics applications. The smallest footprints so far have been achieved in suspended LN photonic crystal nanobeams, with Q factors as high as 1.34×10^5 and a tunability of 16 pm/V in reflection.[22] The reflection mode of operation reduces the sensitivity to waveguide losses and
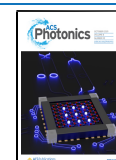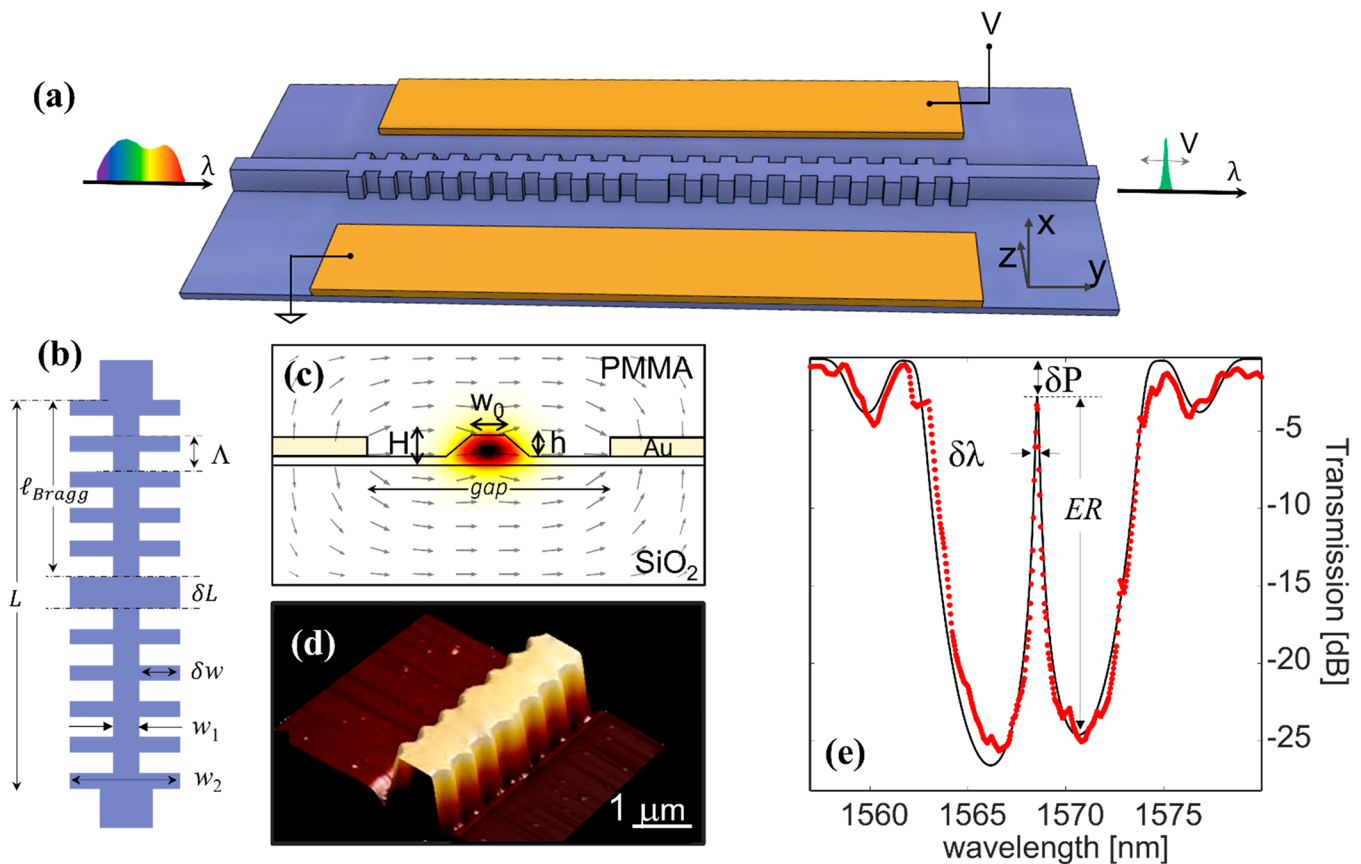
Figure 1. (a) Schematic of a phase-shifted Bragg grating (PSBG) device implemented in a sidewall-modulated LNOI waveguide. x, y, and z are the LN crystal axes. (b) Top view highlighting key parameters of the structure. (c) Cross-sectional view of the waveguide with computed transverse distribution of the optical TE_{00} mode at $\lambda = 1550$ nm (color map) and of the electrostatic field (arrows), for $w_0 = 650$ nm, $H = 500$ nm, $h = 300$ nm, and an electrode gap of 4 μm. (d) Etched PSBG structure imaged by atomic force microscopy. (e) Measured (red markers) and simulated (solid line) transmission spectra of a π-PSBG device. LN waveguide: $w_0 = 450$ nm, $\delta w = 250$ nm, $H = 500$ nm, and $h = 360$ nm. Grating: $\Lambda = \delta L = 435$ nm and 78% duty cycle. Propagation loss: $\alpha = 2.9$ dB/cm.

avoids the need for critical coupling, resulting in much narrower spectral resonances than in transmission for the very same device.[14,21] Moreover, photonic crystal nanobeams need sophisticated etching and a suspended thin LN membrane for EO operation, which might not be ideal in terms of mechanical stability, reproducibility, and scalability of the device fabrication process. On the other hand, they provide the smallest footprints, with good extinction ratios and high EO tunability, enabling advanced functionalities.[22] Sidewall-modulated photonic nanowires (Figure 1) provide an excellent compromise in terms of process scalability and compactness.[3,4] When used for on-chip rejection filters, they can afford very high extinction ratios, which makes them interesting for demanding applications in integrated quantum photonics.[31]

On-chip integrated Bragg gratings (BG) realized in LNOI afford performances comparable to silicon photonics, featuring rejection bandwidths of ~10 nm, extinction ratios as high as 65 dB and enhanced EO tunability on the photonic bandgap edges ($\sigma_\lambda = 23.4$ pm/V).[15,16,20,32] However, they act as notch filters in transmission. Moreover, just as for BGs in silicon photonics, achieving subnanometric bandwidths in them is challenging, due to the high coupling strengths (κ) of the sidewall modulated gratings.[33−35] Such limitations can be overcome by phase-shifted BG (PSBG) structures.[20,36] Nevertheless, similar to 2D resonators,[28] PSBGs feature a trade-off between bandwidth and power penalty, which requires critical

coupling designs for their optimal performance as narrowband filters in transmission.

Here we present a comprehensive experimental study, supported by theoretical analyses, on sidewall modulated PSBG devices in LNOI nanophotonic wires, demonstrating ultranarrowband transmission bandwidths for devices operated at critical coupling in the telecom range. We consider both π-phase-shifted (quarter-wavelength) and longer cavity designs, enabling spectral filtering with single and multi- wavelength transmission. In them, we achieve transmission bandwidths of 14.4 and 8.8 pm ($Q = 1.06 \times 10^5$ and 1.76×10^5), respectively. Moreover, in full agreement with theoretical expectations, we demonstrate enhanced EO spectral tunability ($\sigma_\lambda = 25.1$ pm/V) and record on/off ratios of the optical transmission as a function of the applied voltage, amounting to $\sigma_T = 2.1$ dB/V. The optical contrast is 10.5 dB for CMOS-compatible voltages. Besides providing further confirmation for the degree of maturity reached by the LNOI BG technology platform, the results pave the way for its effective deployment for coherent spectral manipulation of photons in ultrasmall-footprint and low-consumption devices for a broad range of applications, spanning from reconfigurable optical signal processing in telecommunications to programmable quantum optics, microwave photonics, and optical sensing.

DEVICE OVERVIEW

Figure 1a is a sketch of the overall device structure, implemented with nanophotonic waveguides in x-cut LNOI wafers (NANOLN Ltd.) and designed for operation with quasi-TE$_{00}$ modes at telecom wavelengths. Integrated BGs are realized by modulating the nanowire width between the values $w_1 = w_0 - \delta w$ and $w_2 = w_0 + \delta w$, with a constant period Λ. Each PSBG device has a total length L, made of a central segment of length δL and two uniform BG sections of length l_{Bragg} (Figure 1b). The waveguide consists of a LN rib (top-width w_o, height h, sidewall angle θ) etched in a LN slab (original thickness H), clad on top by PMMA and on the bottom by SiO$_2$. EO tuning is achieved by electrodes deposited to the sides of the waveguide, as seen in Figure 1c. The figure also shows the computed transverse profile of the optical TE$_{00}$ mode guided in the rib and the electrostatic field distribution (arrows) generated by a unitary voltage applied to the electrodes. Figure 1d shows the detail of a PSBG structure, fabricated by the process described in Methods. The optical transmission of a π-phase-shifted Bragg grating (π-PSBG), measured as a function of wavelength (λ), is plotted in Figure 1e (markers), together with the result of simulations (solid line) based on the coupled-mode theory (CMT) model detailed in Supporting Information, section S2. Theory and experiments exhibit excellent agreement, showing the level of control achieved in fabrication. On the same plot we highlight the key figures of merit for the transmission filter, that is, its peak wavelength, λ_0; 3 dB bandwidth, $\delta\lambda$; extinction ratio, ER; and power penalty, δP. In a π-PSBG device $\delta L = \Lambda$, yielding only a single transmission peak. Longer phase-shifting segments, $\delta L \gg \Lambda$, can accommodate multiple spectral resonances in the photonic bandgap. They are referred to as *long-cavity* PSBG devices in what follows.

CAVITY MODEL

To design and analyze the response of the PSBG devices we used a guided-wave coupled-mode theory (CMT) approach, which, at a difference with commonly adopted models,[34,35] allows an accurate prediction of the grating coupling coefficient κ (cm^{-1}) in sidewall modulated waveguides. This affords a marked computation speedup over alternative methods (e.g., finite difference time domain) and provides a powerful tool to map the PSBG response over the large parameter space encompassed by the waveguide and grating properties. More details on the CMT model can be found in Supporting Information (section S2). A simple 1D Fabry−Perot cavity model (Supporting Information, section S3),[2] provides further insights and qualitative guidelines for optimization, briefly discussed in this section.

The spectral response of a PSBG device stems from the trapping of light (at λ_0) in a cavity centered around the grating defect δL. The linewidth $\delta\lambda$ of the spectral resonance is inversely proportional to the loaded quality factor (Q) of such a cavity. In the most general case one can write[28,36]

$$\frac{\delta\lambda}{\lambda_0} = \frac{1}{Q} = \frac{1}{Q_\alpha} + \frac{1}{Q_\kappa} \qquad (1)$$

The factor Q_α depends only on the intrinsic losses of the cavity. In our case, the latter are quantified by the waveguide propagation loss coefficient α (cm^{-1}) and are essentially determined by sidewall scattering.[12,37] The term Q_κ expresses the extra loss associated with coupling light into and out of the

cavity, which in our case occurs by transmission through Bragg grating mirrors of length l_{Bragg} (Figure 1b). The transmission of the mirrors depends on κ, hence, Q_κ is parametrized in terms of the latter.

For a given value of the waveguide losses, Q_α is fixed, and according to eq 1, the transmission bandwidth $\delta\lambda$ is minimized by maximizing Q_κ. However, there is a trade-off between increasing Q_κ to decrease $\delta\lambda$ and coupling light efficiently in and out of the cavity, which directly affects the peak power penalty δP. This can be explained by considering that the peak transmission results from the portion of light that reaches δL through the first Bragg mirror, gets trapped in the cavity, and then leaks out through the second Bragg mirror. When the mirror reflectivity is unity, the last term in eq 1 goes to zero, but so does the transmission, yielding infinite power penalty. Qualitatively, one can conclude that there is an optimum value of the mirror reflectivity, which can minimize both $\delta\lambda$ and δP. This occurs for $Q_\alpha \sim Q_\kappa$,[3,38] a condition which we shall designate here as critical coupling, drawing an analogy to the case of ring resonators.[28] In practice, to attain the lower bandwidth limit without compromising the peak transmission, a very fine balance between the intrinsic losses and the reflectivity of the Bragg mirrors has to be hit, requiring careful device optimization (Supporting Information, sections S3 and S4). Similar considerations apply to long-cavity PSBG devices, where the length of the phase-shifting element δL provides an additional control knob to tune the value of Q_κ (Supporting Information, Figure S3). This can alleviate constraints associated with tuning the Bragg mirror reflectivity to achieve critical coupling in π-PSBG devices. On the other hand, increasing δL increases the device footprint. It also decreases the cavity free spectral range (FSR) and may introduce multiple resonances. The ensuing multiwavelength response and the spectral engineering capabilities afforded by long-cavity PSBG devices can on the other hand be appealing for advanced manipulation in several classical and quantum optics applications.[12,39,40] A theoretical analysis of the trade-offs and optimization of PSBG devices is provided in the Supporting Information, section S3. In what follows, we deal with these aspects from an experimental perspective (see also Supporting Information, section S5).

EXPERIMENTAL TRADEOFFS

Figure 2 illustrates the impact of the modulation depth δw of the Bragg gratings (Figure 1b) on the response of π-PSBG devices, that is, the figures of merit $\delta\lambda$, Q, δP, and ER in Figure 1e.

Figure 2a and b plot the peak transmission bandwidths and the loaded quality factors, respectively, for δw varying from 50 to 370 nm, considering otherwise identical π-PSBG devices. Figure 2c and d illustrate the evolution of the power penalty and extinction ratio, respectively. The circles are experimental data, while the solid lines are numerical predictions obtained with the CMT model. The simulations assume a constant loss coefficient, independent of δw and equal to the one measured on unmodulated waveguides, $\alpha_0 = 2.9$ dB/cm in this case.

For values of δw up to 240 nm, the experiments feature a monotonic bandwidth decrease (Q factor increase), which is fully consistent with theory. However, beyond that point the transmission bandwidth saturates at $\delta\lambda \sim 115$ pm (Figure 2a), corresponding to $Q = 1.37 \times 10^4$ (Figure 2b), in contrast with theory (solid line), which predicts a minimum bandwidth of 26
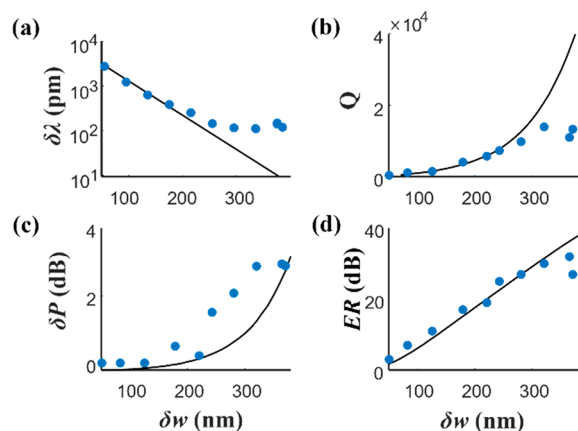
Figure 2. (a) Peak transmission bandwidth, (b) loaded Q factor, (c) power penalty, and (d) extinction ratio, plotted as a function of the sidewall modulation amplitude δw in π-PSBG devices. Filled circles: measurements. Solid lines: simulations for a fixed loss value: $\alpha = 2.9$ dB/cm. Other parameters: $w_0 = 450$ nm, $L = 217$ μm, $\Lambda = 435$ nm, $H = 500$ nm, and $h = 360$ nm. See Supporting Information, Figure S6, for the measured and simulated spectra.

pm. The experimental results also indicate significant power penalties and degradation of the peak extinction ratio. These effects exhibit strong similarities with the ones previously reported for BG devices on other nanophotonic platforms,[34] and point out to the additional non-negligible losses introduced by the sidewall modulation in PSBG devices for $\delta w > 200$ nm. The additional loss induced by the grating sidewall modulation (α_{BG}) can be quantitatively evaluated via the CMT model through fits on the experimental spectra assuming $\alpha = \alpha_0 + \alpha_{BG}$, with α_{BG} as the fitting parameter. The inferred loss values added by the grating ranged between 3 and 10 dB/cm, for δw between 240 and 370 nm (see also Supporting Information, section S6).

The detrimental impact of scattering losses sets an upper bound to the possibility to attain the narrowest linewidths uniquely by increasing δw. However, since Q_κ depends on the normalized quantity κl_{Bragg}, the π-PSBG device response can be further tuned by adjusting l_{Bragg} and, hence, the device length L. This approach is illustrated in Figure 3. The 2D histogram of Figure 3 shows the loaded Q factors measured for a set of 27 waveguides, made on the same chip and encompassing three different values of L (105–420 μm) and nine of δw (82–370 nm). The shortest gratings correspond to cavities that are strongly undercoupled for all modulation

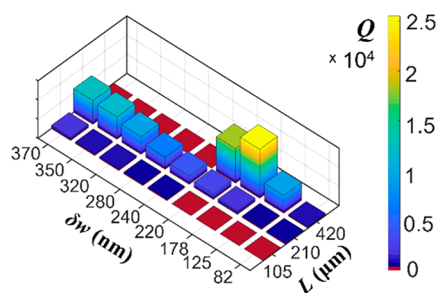**Figure 3.** Experimental 2D tomography of the loaded quality factors of π-PBSG waveguides as a function of sidewall corrugation depth (δw) and total device length (L), for $w_0 = 650$ nm, $H = 500$ nm, $h = 360$ nm, and $\Lambda = 420$ nm.

depths. Doubling the device length ($L = 210$ μm) yields a monotonic increase of the Q factor with δw. However, it does not reach critical coupling. With a further increase of the device length to $L = 420$ μm, a critical coupling regime is achieved for $\delta w < 200$ nm, that is, at working points where the sidewall modulation does not add significant extra loss. For $L = 420$ μm, Q features a nonmonotonic trend as a function of δw, with a peak ($Q = 2.6 \times 10^4$) at $\delta w = 178$ nm, corresponding to a measured transmission bandwidth $\delta\lambda = 59$ pm, a power penalty of 3 dB and an extinction ratio of 25 dB.

Finally, besides a careful choice of δw and L, the optimization of both π-PSBG and long-cavity devices involves the overall minimization of the waveguide propagation losses on the LNOI platform. This was achieved through suitable design and fabrication, targeting a nanowire width $w_0 \sim 650$ nm and etching depths $h \sim 300$ nm, offering a good compromise between modal confinement, propagation losses, grating coupling strengths, and device footprint (Supporting Information, Table S5). As an indication, a propagation loss value of 1.5 dB/cm yields a theoretical limit of $Q = 1.1 \times 10^5$ for critically coupled π-PSBG devices (see also Supporting Information, section S4, for further quantification).

■ NARROWBAND TRANSMISSION

The best results in terms of narrowband devices are highlighted in Figure 4a and Figure 4b, with reference to π-PSBG and long cavity devices, respectively.
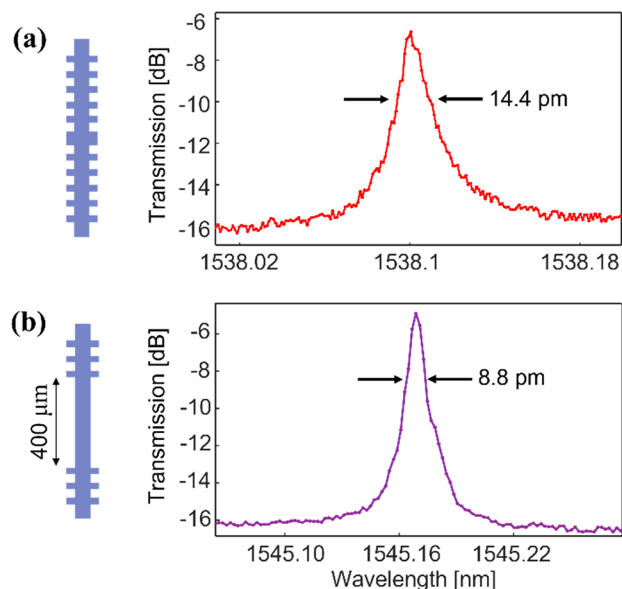

Figure 4. Transmission peaks measured near critical coupling in a (a) π-PSBG device with $l_{Bragg} = 340$ μm, $\delta L = 425$ nm, and (b) long cavity device with $l_{Bragg} = 273$ μm, $\delta L = 400$ μm. $H = 500$ nm, $h = 310$ nm, $w_0 = 640$ nm, $\delta w = 100$ nm, and $\Lambda = 425$ nm in both cases.

Critically coupled devices with loaded Q-factors in excess of 10^5 were consistently achieved for π-PSBG devices, in good agreement with theoretical predictions. An example is provided in Figure 4a, showing the spectrum of the transmission peak from a 680 μm long π-PSBG with a sidewall modulation depth of 100 nm, exhibiting a bandwidth of 14.4 pm ($Q = 1.06 \times 10^5$), with an ER of ~9 dB. Long-cavity PSBG designs yielded even narrower bandwidths. This is illustrated by Figure 4b for a device with $\delta L = 400$ μm, featuring a bandwidth $\delta\lambda = 8.8$ pm

($Q = 1.76 \times 10^5$) and an ER of ~11 dB. To the best of our knowledge, this is the narrowest peak ever reported on this kind of 1D resonator on LN.

The full extent of the multipeaked spectral response measured in the long cavity PSBG devices is shown in Figure 5, where we show the evolution of the PSBG transmission
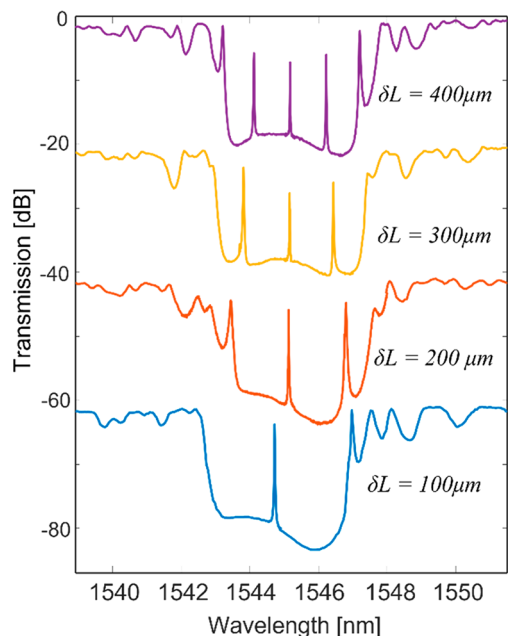

Figure 5. Measured transmission spectra on long cavity devices for δL = 100, 200, 300, and 400 μm. Otherwise, all parameters are the same as in Figure 4b, which shows a spectral zoom-in of the central peak on the violet curve.

spectra for four different cavity lengths δL, comprised between 100 and 400 μm. As δL is increased, the number of transmission peaks within the bandgap increases as a result of a progressive decrease in the FSR. For the shortest cavity, that is, δL = 100 μm, the FSR is almost identical to half the width of the photonic bandgap (FSR = 2.25 nm), yielding a single peak around the Bragg wavelength, with a transmission bandwidth $\delta \lambda$ = 10.4 pm ($Q \sim 1.49 \times 10^5$). On the other end, for δL = 400 μm, the FSR reaches a value of 1.06 nm, yielding three transmission peaks located well within the photonic bandgap. Each of them features comparable bandwidths to the one highlighted in Figure 4b. The smallest power penalty is obtained for δL = 100 μm and amounts to δP = 1.95 dB.

◼ ELECTRO-OPTIC TUNING

The transmission peak can be tuned through the additional application of a voltage to electrodes deposited by the sides of the LNOI waveguide (see also Supporting Information, section S8).[15,16] When a positive voltage is applied to the $+z$ side of the LN rib, the Bragg resonance wavelength experiences a red shift. A record tunability of $\sigma_\lambda = \partial \lambda / \partial V$ = 25.1 pm/V was measured on optimized π-PSBG devices, with 680 μm long side electrodes. Long cavity devices with δL = 200 μm yielded a value of 17 pm/V. The short cavity length of π-PSBG devices ($\delta L = \Lambda$) requires the application of the tuning voltage along the full length of the device (sketch in Figure 6a) in order to build up a sufficiently high EO phase shift and move the transmission peak across its spectral width. Since the voltage is applied also to the Bragg grating sections (l_{Bragg}), the photonic
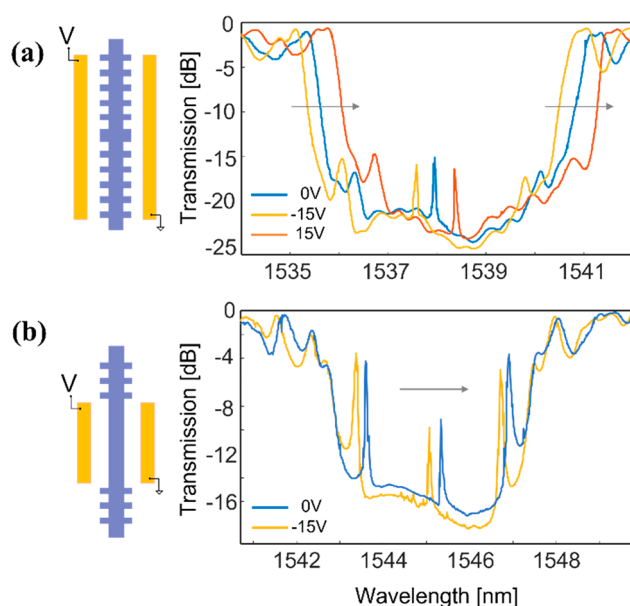

Figure 6. Optical transmission curves of a (a) π-PSBG and (b) long cavity (δL = 200 μm) device, measured at voltages of −15, 0, and 15 V (yellow, blue, and orange curves) applied to the electrodes. The sketches on the left highlight the location of the latter with respect to the PSBG grating in the two cases.

bandgap is spectrally shifted together with the transmission peak (arrows in Figure 6a), as in ordinary BG devices.[4,16] The yellow, blue, and red curves in Figure 6a illustrate the full spectral responses of a π-PSBG, measured at −15, 0, and 15 V, respectively.

The features of the photonic bandgap spectrum far from the resonance peak get deformed as one applies a voltage to the electrodes. Similar distortions have been observed elsewhere in BG devices operating at the band edges,[16] and limit the tuning performance especially at low operating voltages. Such spectral perturbations are essentially absent in the tuning of the transmission peak. Furthermore, its ultranarrow bandwidth is particularly advantageous for achieving high transmission contrasts at low voltages. In this respect a meaningful figure of merit is the change in device transmission per unit voltage, expressed by the coefficient $\sigma_T = ER/\tilde{V}$, where $\tilde{V}$ is the voltage to be applied in order to induce a transmission change equal to the peak extinction ratio, that is, $\Delta T(\tilde{V})$ = ER. For the π-PSBG device of Figure 6a, σ_T amounts to 0.6 dB/V. This performance is further improved with long cavity devices. In this case, the voltage is applied only to the central segment of length δL (and not to the Bragg grating sections). This shifts the transmission peaks in the photonic bandgap without affecting the spectral location of the latter, as apparent from Figure 6b. An applied voltage of 5 V shifts the transmission peak by ~85 pm with negligible spectral distortion (see also Supporting Information, Figure S10), yielding a transmission change of 10.5 dB at the original Bragg wavelength λ = 1544.96 nm. This corresponds to a spectral tunability σ_λ = 17 pm/V and a transmission modulation efficiency σ_T = 2.1 dB/V. The latter improves by more than one order of magnitude on previous results achieved in the static tuning of LNOI Bragg gratings (0.14 dB/V).[16] The analysis of the measurements performed on the very same PSBG devices before and after adding the electrodes (process steps described in Methods) indicates an extra loss of ~6 dB/cm due to combined effects of

Table 1. Representative EO Tunable Filters Based on Thin Film LiNbO₃

platf.	archit.[a]	config.	footprint (μm^2)	Q (×10⁵)	ER (dB)	δP (dB)	FSR (nm)	σ_λ (pm/V)	σ_T (dB/V)	ref.
LNOI	ring/racetrack	through port	40000	50	~15[b]		5[b]			24
LNOI	ring/racetrack	through port	25000[b]	7	~12[b]		3[b]	2.4[b]		26
Si-LN	ring resonator	through port	400	1.6	~3.8[b]		4.9			27
Si-LN	ring resonator	through port	1600	0.14	~11.5[b]			3.3	0.8[b]	23
Si-LN	1D ph. crystal	transmission	30	1.2	~13[b]	~17[b]		1–2[b]	<0.5[b]	27
LNOI	1D ph. crystal	reflection	50	1.34	~11.5[b]			16		21
LNOI	SWM wire	transmission	1000	0.2	~15[b]	~0[b]	1[b]	15.7		44
LNOI	SWM wire	transmission	400	0.34	~7.5[b]	7.5[b]		14.6	~1[b]	15
LNOI	SWM wire	trans. π-PSBG	490	1(0.4)	12(10)	6(15)		-(25)	-(0.6)	this work
		long-cavity	700	1.76(0.4)	11(10.5)	6(7.5)	1(1)	-(17)	-(2.1)	

[a]SWM = sidewall-modulated. [b]Not quoted, but extrapolated with simulations from the available data in the paper. The last two rows quote the values for passive devices and, within brackets, those for active devices.

reprocessing the PMMA cladding (+3 dB/cm) and depositing the metal electrodes (+3 dB/cm). The ensuing power penalty is particularly severe for π-PSBG devices, which become strongly overcoupled. The added loss can potentially be eliminated by replacing the PMMA cladding with SiO₂ and skipping the extra fabrication steps required for optical diagnostics prior to electrode patterning. An improved process for electrode deposition is expected to bring the power penalties seen in Figure 6 back to the values for critical coupling ($\delta P \sim 6$ dB) and further boost the EO transmission tunability to $\sigma_T = 4.66$ dB/V. The degradation induced by the PMMA and electrode patterning process can be appreciated from the data in Table 1, where we list key performance indicators for our devices in the last two rows and indicate in brackets the parameter values measured after adding the electrodes. Despite such a degradation, the PSBG devices still provide an excellent EO performance, featuring the highest value of σ_λ (25.1 pm/V) and the best transmission tunability σ_T in the table. Prior to electrode deposition, our passband filters exhibit Q values en par with the best notch filters in 1D photonic crystals and 2D ring/racetrack resonators in the table, with the exception of the ultralow loss devices corresponding to the first row of Table 1 (0.03 dB/cm). However, as discussed in the introduction, those resonators (ref 24) operate as rejection filters. The Q factor is therefore not constrained by transmission penalty trade-offs. In fact, the Q values reported in this work are already at the limit of the performance expected from the PSBG architecture while still keeping reasonably small device footprints (and large FSR), as further discussed in section S3 of Supporting Information.

CONCLUSIONS

We reported a systematic study on phase shifted Bragg gratings (PSBG) for electrically tunable integrated ultranarrow bandpass filters in thin film lithium niobate, encompassing theory and experiments. We considered both π phase-shifted (π-PSBG) and long-cavity configurations implemented in sidewall-modulated nanowire waveguides with average widths of ~650 nm. The full mapping of the waveguide and grating parameter space highlighted key elements for device optimization to achieve narrowband responses without compromising transmission (i.e., critical coupling). The analyses allowed us to identify critical trade-offs in device fabrication and design on this specific device architecture and technology platform. With sidewall modulations $\delta w \sim 100$ nm, we achieved experimentally the theoretical limit for critically coupled π-PSBG, measuring transmission bandwidths of 14.4

pm ($Q \sim 10^5$) on devices with a footprint of only 490 μm^2. Good agreement between theory and experiments was also demonstrated for multiwavelength resonant devices implemented with long cavities ($\delta L \sim 100-400$ μm), yielding bandwidths of 8.8 pm and loaded Q factors of 1.76×10^5. The transmission penalties measured on critically coupled devices (~6 dB) agreed also well with predictions. The rich parameter space affords the possibility to achieve zero penalty operation near the critical coupling points, at the price of slightly larger bandwidths (32 pm measured on long cavity devices, see also Supporting Information, Figure S5). Finally, by exploiting the electro-optic effect, we achieved a tunability of the transmission wavelength of 25.1 pm/V and an optical transmission contrast at the Bragg wavelength of ~10.5 dB at CMOS-compatible voltages. Despite a partial degradation of the narrowband features induced by the electrode patterning process, the PSGB devices afforded a record electro-optic tunability, of 2.1 dB/V. The work demonstrates devices well-suited for fine spectral manipulation in single and multi-wavelength regimes with low-consumption electrical reconfigurability. These results hold promise for further applications of integrated LNOI photonic circuits to electro-optic switching and modulation in telecommunication systems as well as efficient photon manipulation in integrated quantum photonics. Moreover, they pave the way to the implementation of more advanced functionalities for spectral shaping and tuning, such as superstructured gratings for dispersion engineering and $\chi^{(2)}$ nonlinearity enhancement for novel frequency comb or quantum sources.[12,40] The small footprints and low-voltage operation achieved with these devices and the scalability of their fabrication process might also be advantageously exploited toward developments of microwave photonics and programmable nanophotonics for, for example, multispectral sensing, neuromorphic, and quantum computing.[4,41−43]

METHODS

A previously developed fabrication process,[32] was optimized for improved reproducibility and fine patterning resolutions with deeper LNOI etching. All the integrated nanophotonic components were simultaneous defined on chip by a single-step electron beam exposure (Raith Voyager, acceleration voltage 50 kV), patterning a resist layer (ma-N2400) spun on a chromium layer deposited on commercial x-cut LNOI chips (NANOLN Ltd.). The chromium was patterned by Cl₂/O₂ reactive ion etching (Oxford Plasmalab 100) and used as a hard mask for subsequent Ar⁺ ion milling of the underlying LN film. The process yielded nanowire waveguides with sidewall

angles of 55−65°, which were clad with a 2 μm thick layer of PMMA (MicroChem 950) baked at 170 °C, to perform optical measurements prior to electrode deposition.[19,20] For the latter, the PMMA cladding layer was first stripped off the chip. Then the tuning electrodes were patterned (with new PMMA lithography) by liftoff of a 50 nm thick Au layer with a 10 nm thin Cr adhesion layer. Finally, a new PMMA cladding layer was deposited on the chips.

The optical characterizations were performed by coupling light from single mode optical fibers at telecom wavelengths into the LNOI chip with integrated grating couplers and tapers for selective excitation of the fundamental TE$_{00}$ mode in the PSBG nanowires. As in previous work,[32] we used a tunable continuous-wave laser source (Yenista T100S) for spectrally resolved measurements. The device throughput was recorded off-chip with a fiber-coupled power meter (Newport 2931-C) synchronized with the laser.

Numerical analyses of the waveguide modes in the wavelength range of interest (λ = 1500−1600 nm) and of the electrostatic field distributions generated by the electrodes were performed with a commercial finite element vectorial solver (COMSOL). The PSBG spectral response was investigated with a coupled mode theory approach implemented with own codes in MATLAB. Further details are provided in the Supporting Information.

ASSOCIATED CONTENT

Ⓢ Supporting Information

The Supporting Information is available free of charge at https://pubs.acs.org/doi/10.1021/acsphotonics.1c00383.

> Nomenclature; Coupled mode theory; Fabry−Perot cavity model; Critical coupling assessment; Experimental trade-offs; Extra-loss penalty for large sidewall modulation; Effective cavity length; Electro-optic tuning (PDF)

AUTHOR INFORMATION

Corresponding Author

Katia Gallo − *Department of Applied Physics, KTH Royal Institute of Technology, Stockholm SE-106 91, Sweden;* ⓞ orcid.org/0000-0001-7185-0457; Email: gallo@kth.se

Authors

Alessandro Prencipe − *Department of Applied Physics, KTH Royal Institute of Technology, Stockholm SE-106 91, Sweden;* ⓞ orcid.org/0000-0002-3889-6223

Mohammad Amin Baghban − *Department of Applied Physics, KTH Royal Institute of Technology, Stockholm SE-106 91, Sweden;* Present Address: Currently with AFRY AB, Frösundaleden 2A, Solna SE-169 99, Sweden; ⓞ orcid.org/0000-0001-7242-7300

Complete contact information is available at:
https://pubs.acs.org/10.1021/acsphotonics.1c00383

Author Contributions

K.G., A.P., and M.A.B. conceived the study, A.P. fabricated and characterized the devices, with contributions by M.A.B. A.P. and K.G. performed the design, modeling, and data analysis and wrote the manuscript. All authors approved the final version of the manuscript.

Notes

The authors declare no competing financial interest.

ACKNOWLEDGMENTS

REFERENCES

(1) Nishihara, H.; Haruna, M.; Suhara, T. *Optical Integrated Circuits*; McGraw-Hill, 1989; p 46.

(2) Yariv, A.; Yeh, P. *Photonics: Optical Electronics in Modern Communications*; Oxford University Press, 2007; pp 183−184 and 450−458.

(3) Kaushal, S.; Cheng, R.; Ma, M.; Mistry, A.; Burla, M.; Chrostowski, L.; Azaña, J. Optical signal processing based on silicon photonics waveguide Bragg gratings: review. *Front. Optoelectron.* **2018**, *11*, 163−188.

(4) Zhang, W.; Yao, J. A fully reconfigurable waveguide Bragg grating for programmable photonic signal processing. *Nat. Commun.* **2018**, *9*, 1396.

(5) Alferness, R. C.; Joyner, C. H.; Divino, M. D.; Buhl, L. L. InGaAsP/InP waveguide grating filters for λ=1.5 μm. *Appl. Phys. Lett.* **1984**, *45*, 1278−1280.

(6) Kogelnik, H.; Shank, C. V. Coupled-Wave Theory of Distributed Feedback Lasers. *J. Appl. Phys.* **1972**, *43*, 2327−2335.

(7) Ouellette, F. Dispersion cancellation using linearly chirped Bragg grating filters in optical waveguides. *Opt. Lett.* **1987**, *12*, 847−849.

(8) Hernandez, V. J.; Bennett, C. V.; Moran, B. D.; Drobshoff, A. D.; Chang, D.; Langrock, C.; Fejer, M. M.; Ibsen, M. 104 MHz rate single-shot recording with subpicosecond resolution using temporal imaging. *Opt. Express* **2013**, *21*, 196−203.

(9) Lee, K. J.; Liu, S.; Parmigiani, F.; Ibsen, M.; Petropoulos, P.; Gallo, K.; Richardson, D. J. OTDM to WDM format conversion based on quadratic cascading in a periodically poled lithium niobate waveguide. *Opt. Express* **2010**, *18*, 10282−10288.

(10) Lova, P.; Manfredi, G.; Bastianini, C.; Mennucci, C.; Buatier de Mongeot, F.; Servida, A.; Comoretto, D. Flory-Huggins Photonic Sensors for the Optical Assessment of Molecular Diffusion Coefficients in Polymers. *ACS Appl. Mater. Interfaces* **2019**, *11*, 16872−16880.

(11) Pooley, J.; Price, E.; Ferguson, J. W.; Ibsen, M. Optimised Chirped Fibre Bragg Gratings for Detonation Velocity Measurements. *Sensors* **2019**, *19*, 3333.

(12) Xie, S.; Zhang, Y.; Hu, Y.; Veilleux, S.; Dagenais, M. On-Chip Fabry-Perot Bragg Grating Cavity Enhanced Four-Wave Mixing. *ACS Photonics* **2020**, *7*, 1009−1015.

(13) Falah, A. A. S.; Mokhtar, M. R.; Yusoff, Z.; Ibsen, M. Reconfigurable Phase-Shifted Fiber Bragg Grating Using Localized Micro-Strain. *IEEE Photonics Technol. Lett.* **2016**, *28*, 951−954.

(14) Pohl, D.; Kaufmann, F.; Escalé, M. R.; Holzer, J.; Grange, R. Tunable Bragg Grating Filters and Resonators in Lithium Niobate-on-Insulator Waveguides. *Conference on Lasers and Electro-Optics (CLEO 2020)*, IEEE, 2020; paper STu4J.5.

(15) Pohl, D.; Messner, A.; Kaufmann, F.; Escalé, M. R.; Holzer, J.; Leuthold, J.; Grange, R. 100-GBd Waveguide Bragg Grating Modulator in Thin-Film Lithium Niobate. *IEEE Photonics Technol. Lett.* **2021**, *33*, 85−88.

(16) Escalé, M. R.; Pohl, D.; Sergeyev, A.; Grange, R. Extreme electro-optic tuning of Bragg mirrors integrated in lithium niobate nanowaveguides. *Opt. Lett.* **2018**, *43*, 1515−1518.

(17) Xu, M.; He, M.; Liu, X.; Pan, Y.; Yu, S.; Cai, X. Integrated Lithium Niobate Modulator and Frequency Comb Generator Based

on Fabry-Perot Resonators. *Conference on Lasers and Electro-Optics (CLEO 2020)*, IEEE, 2020; paper JTh2B.27.

(18) Zhang, G.; Haw, J. Y.; Cai, H.; Xu, F.; Assad, S. M.; Fitzsimons, J. F.; Zhou, X.; Zhang, Y.; Yu, S.; Wu, J.; Ser, W.; Kwek, L. C.; Liu, A. Q. An integrated silicon photonic chip platform for continuous-variable quantum key distribution. *Nat. Photonics* **2019**, *13*, 839−842.

(19) Prencipe, A.; Baghban, M. A.; Gallo, K. Ultra-narrowband Bragg grating filters in LiNbO₃ on insulator photonic wires. *OSA Advanced Photonics Congress (AP 2020)*, OSA, 2020; paper IW2A.5.

(20) Baghban, M. A.; Gallo, K. Phase-Shifted Bragg Grating Resonators in Thin-Film Lithium Niobate Waveguides. *Conference on Lasers and Electro-Optics (CLEO 2019)*, IEEE, 2019; paper SF2J.7.

(21) Liang, H.; Luo, R.; He, Y.; Jiang, H.; Lin, Q. High-quality lithium niobate photonic crystal nanocavities. *Optica.* **2017**, *4*, 1251−1258.

(22) Li, M.; Ling, J.; He, Y.; Javid, U. A.; Xue, S.; Lin, Q. Lithium niobate photonic-crystal electro-optic modulator. *Nat. Commun.* **2020**, *11*, 4123.

(23) Chen, L.; Xu, Q.; Wood, M. G.; Reano, R. M. Hybrid silicon and lithium niobate electro-optical ring modulator. *Optica.* **2014**, *1*, 112−118.

(24) Zhang, M.; Wang, C.; Cheng, R.; Shams-Ansari, A.; Lončar, M. Monolithic ultra-high-Q lithium niobate microring resonator. *Optica.* **2017**, *4*, 1536−1537.

(25) Wang, C.; Zhang, M.; Chen, X.; Bertrand, M.; Shams-Ansari, A.; Chandrasekhar, S.; Winzer, P.; Lončar, M. Integrated lithium niobate electro-optic modulators operating at CMOS-compatible voltages. *Nature* **2018**, *562*, 101−104.

(26) Wang, C.; Zhang, M.; Yu, M.; Zhu, R.; Hu, H.; Loncar, M. Monolithic lithium niobate photonic circuits for Kerr frequency comb generation and modulation. *Nat. Commun.* **2019**, *10*, 978.

(27) Witmer, J. D.; Valery, J. A.; Arrangoiz-Arriola, P.; Sarabalis, C. J.; Hill, J. T.; Safavi-Naeini, A. H. High-Q photonic resonators and electro-optic coupling using silicon-on-lithium-niobate. *Sci. Rep.* **2017**, *7*, 46313.

(28) Bogaerts, W.; De Heyn, P.; Van Vaerenbergh, T.; De Vos, K.; Kumar Selvaraja, S.; Claes, T.; Dumon, P.; Bienstman, P.; Van Thourhout, D.; Baets, R. Silicon microring resonators. *Laser Photonics Rev.* **2012**, *6*, 47−73.

(29) Zhang, M.; Wang, C.; Kharel, P.; Zhu, D.; Lončar, M. Integrated lithium niobate electro-optic modulators: when performance meets scalability. *Optica.* **2021**, *8*, 652−667.

(30) Zhu, D.; Shao, L.; Yu, M.; Cheng, R.; Desiatov, B.; Xin, C. J.; Hu, Y.; Holzgrafe, J.; Ghosh, S.; Shams-Ansari, A.; Puma, E.; Sinclair, N.; Reimer, C.; Zhang, M.; Lončar, M. Integrated photonics on thin-film lithium niobate. *Adv. Opt. Photonics* **2021**, *13*, 242−352.

(31) Harris, N. C.; Grassani, D.; Simbula, A.; Pant, M.; Galli, M.; Baehr-Jones, T.; Hochberg, M.; Englund, D.; Bajoni, D.; Galland, C. Integrated Source of Spectrally Filtered Correlated Photons for Large-Scale Quantum Photonic Systems. *Phys. Rev. X* **2014**, *4*, 041047.

(32) Baghban, M. A.; Schollhammer, J.; Errando-Herranz, C.; Gylfason, K. B.; Gallo, K. Bragg gratings in thin-film LiNbO3 waveguides. *Opt. Express* **2017**, *25*, 32323−32332.

(33) Wang, X.; Shi, W.; Yun, H.; Grist, S.; Jaeger, N. A. F.; Chrostowski, L. Narrow-band waveguide Bragg gratings on SOI wafers with CMOS-compatible fabrication process. *Opt. Express* **2012**, *20*, 15547−15558.

(34) Spencer, D. T.; Davenport, M.; Srinivasan, S.; Khurgin, J.; Morton, P. A.; Bowers, J. E. Low kappa, narrow bandwidth Si3N4 Bragg gratings. *Opt. Express* **2015**, *23*, 30329−30336.

(35) Ctyroky, J.; Wangüemert-Pérez, J. G.; Kwiecien, P.; Richter, I.; Litvik, J.; Schmid, J. H.; Molina-Fernandez, I.; Ortega-Moñux, A.; Dado, M.; Cheben, P. Design of narrowband Bragg spectral filters in subwavelength grating metamaterial waveguides. *Opt. Express* **2018**, *26*, 179−194.

(36) Alferness, R. C.; Joyner, C. H.; Divino, M. D.; Martyak, M. J. R.; Buhl, L. L. Narrowband grating resonator filters in InGaAsP/InP waveguides. *Appl. Phys. Lett.* **1986**, *49*, 125−127.

(37) Ji, X.; Barbosa, F. A. S.; Roberts, S. P.; Dutt, A.; Cardenas, J.; Okawachi, Y.; Bryant, A.; Gaeta, A. L.; Lipson, M. Ultra-low-loss on-chip resonators with sub-milliwatt parametric oscillation threshold. *Optica.* **2017**, *4*, 619−624.

(38) Wang, X.; Grist, S.; Flueckiger, J.; Jaeger, N. A. F.; Chrostowski, L. Silicon photonic slot waveguide Bragg gratings and resonators. *Opt. Express* **2013**, *21*, 19029−19039.

(39) Xu, M.; He, M.; Zhang, H.; Jian, J.; Pan, Y.; Liu, X.; Chen, L.; Meng, X.; Chen, H.; Li, Z.; Xiao, X.; Yu, S.; Yu, S.; Cai, X. High-performance coherent optical modulators based on thin-film lithium niobate platform. *Nat. Commun.* **2020**, *11*, 3911.

(40) Yu, S.-P.; Jung, H.; Briles, T. C.; Srinivasan, K.; Papp, S. B. Photonic-Crystal-Reflector Nanoresonators for Kerr-Frequency Combs. *ACS Photonics* **2019**, *6*, 2083−2089.

(41) Marpaung, D.; Yao, J.; Capmany, J. Integrated microwave photonics. *Nat. Photonics* **2019**, *13*, 80−90.

(42) Shastri, B. J.; Tait, A. N.; Ferreira de Lima, T.; Pernice, W. H. P.; Bhaskaran, H.; Wright, C. D.; Prucnal, P. R. Photonics for artificial intelligence and neuromorphic computing. *Nat. Photonics* **2021**, *15*, 102−114.

(43) Wang, J.; Sciarrino, F.; Laing, A.; Thompson, M. G. Integrated photonic quantum technologies. *Nat. Photonics* **2020**, *14*, 273−284.

(44) Xu, M.; He, M.; Zhu, Y.; Liu, L.; Chen, L.; Yu, S.; Cai, X. Integrated thin film lithium niobate Fabry-Perot modulator [Invited]. *Chin. Opt. Lett.* **2021**, *19*, 060003.